



Article

# Graphene Quantum Dots with High Yield and High Quality Synthesized from Low Cost Precursor of Aphanitic Graphite

Shuling Shen \*, Junjie Wang, Zhujun Wu, Zheng Du, Zhihong Tang and Junhe Yang \*

School of Materials Science and Engineering, University of Shanghai for Science and Technology, Shanghai 200093, China; wondry\_wjj@outlook.com (J.W.); zhujun\_wu@sina.com (Z.W.); duzhengduyilin@163.com (Z.D.); zhtang@usst.edu.cn (Z.T.)

\* Correspondence: slshen@usst.edu.cn (S.S.); jhyang@usst.edu.cn (J.Y.)

Received: 22 January 2020; Accepted: 18 February 2020; Published: 21 February 2020



**Abstract:** It is difficult to keep the balance of high quality and high yield for graphene quantum dots (GQDs). Because the quality is uncontrollable during cutting large 2D nanosheets to small 0D nanodots by top-down methods and the yield is low for GQDs with high quality obtained from bottom-up strategy. Here, aphanitic graphite (AG), a low-cost graphite contains a large amount of small graphite nanocrystals with size of about 10 nm is used as the precursor of graphene oxide quantum dots (GO-QDs) for the first time. GO-QDs with high yield and high quality were successfully obtained directly by liquid phase exfoliating AG without high strength cutting. The yield of these GO-QDs can reach up to 40 wt. %, much higher than that obtained from flake graphite (FG) precursor (less than 10 wt. %). The size of GO-QDs can be controlled in 2–10 nm. The average thickness of GO-QDs is about 3 nm, less than 3 layer of graphene sheet. Graphene quantum dots (GQDs) with different surface properties can be easily obtained by simple hydrothermal treatment of GO-QDs, which can be used as highly efficient fluorescent probe. Developing AG as precursor for GQDs offers a way to produce GQDs in a low-cost, highly effective and scalable manner.

**Keywords:** graphene quantum dots; aphanitic graphite; low cost precursor; high yield; high quality

## 1. Introduction

Graphene, with unique thermal, mechanical, and electronic properties, as well as its excellent chemical stability, has attracted increasingly attention in recent years [1–3]. These superior properties of graphene have advanced applications in energy, catalysis, and biomaterial fields [4–9]. However, large graphene nanosheet has zero bandgap which limits its electronic and opto-electronic application [10,11]. According to quantum confinement and edge effect, the bandgap of graphene can be designed by varying its size. GQDs with zero-dimensional structure, higher photo stability, lower toxicity, and easily changeable functional groups have attracted considerable attention for applying in sensors, bioimaging, and solar cell [12–18].

Over the past few years, GQDs have been widely studied and various synthesis methods have been developed [19–21]. These methods can be divided into two types: bottom-up strategy and top-down strategy. As for bottom-up approach, solution-based chemical routes were demonstrated as useful methods to synthesize large polycyclic aromatic hydrocarbons from dendritic arene precursors [22–24]. Li group employed 2',4',6'-triakyl phenyl groups as the precursor to form the edge of graphene moieties [25]. Through this approach, the size and colloidal stability could be controlled. But bottom-up approaches usually contain many complicated steps and the yield of GQDs is low. Furthermore, during the synthesis process, large amount of organic solvents is usually used. The purification

of obtained GQDs is difficult and the purified GQDs cannot be dispersed in water easily, which limit their applications. Comparing with bottom-up strategy, top-down approach is a relatively simple process. The crucial point of this approach is how to cut large 2D nanosheets to small 0D nanodots. Many researchers are committed to developing simple and efficient methods for cutting large sheets into nanodots. Various synthesis routes have been developed, such as oxidation cutting [26], hydrothermal (solvothetical) [27,28], electrochemistry [29–31], photo-Fenton reaction [32], and oxygen plasma etching [33]. Various precursors were adopted, such as graphene oxide (GO) [34], C60 [35], carbon nano-onions [36], carbon fibers [37], coal [38,39], graphite nanoparticle [40], and rice husk [41]. However, there are also many problems that limit the practical application of GQDs, such as complex pretreatments, high energy-consumption, special instruments or high precursor costs, and so on. It is still a challenge to synthesize GQDs or GO-QDs at a large scale with uniform size in a high yield and low-cost way.

Different from coal, AG is a kind of graphite ore that is composed of carbonaceous material by thermal decomposition of deep metamorphic products (such as from coal deterioration). Its conductivity, thermal conductivity, lubricity, and oxidation resistance are lower than full crystalline graphite. Therefore, it has not been taken seriously and its price is much lower than flake graphite. AG with particle size of  $\sim 5 \mu\text{m}$  has been used to synthesize small size graphene sheets [42,43]. But it is ignored that AG contains a large amount of small graphite nanocrystals with size of about 10 nm. Here, reserve thinking of how to cut 2D graphene sheets into 0D nanodots efficiently, we report for the first time the large-scale synthesis of GO-QDs with uniform size by simply exfoliating AG precursor through a chemical exfoliation process without high-strength cutting. The yield of GO-QDs can reach up to 40%, much higher than that by using FG as precursor (less than 10%). GQDs with different surface properties can be easily obtained by simply hydrothermal treating of GO-QDs in the presence of different functional molecules. These modified GQDs can be used as highly efficient fluorescent probe.

## 2. Materials and Methods

### 2.1. Synthesis of GO-QDs by Exfoliating of AG

The exfoliating of AG (Chenzhou Botai Graphite Co., Ltd., Hunan, China) was carried out by a conventional intercalation process, which was generally used for preparing large GO sheets. In a typical procedure, 5 g of AG, 2.5 g of  $\text{NaNO}_3$ , and 115 mL of concentrated  $\text{H}_2\text{SO}_4$  were ultrasonically mixed in a beaker at room temperature for 30 min. Then the beaker was removed into an ice bath under mild agitation and 15 g of  $\text{KMnO}_4$  was added slowly at a temperature under  $10^\circ\text{C}$ . Then the mixture was heated to  $35^\circ\text{C}$  and kept for 40 min. After adding 250 mL of deionized (DI) water, the solution was kept at  $98^\circ\text{C}$  for another 45 min. Then the mixture was diluted to 700 mL and 30 mL of  $\text{H}_2\text{O}_2$  (30%) was added. After that, the solution was centrifuged and washed by DI water for several times until the pH value of the system reached to about 7. Then the as-prepared sample was first centrifuged at 3000 rpm for 15 min, dividing into supernatant and precipitates. The precipitates mainly composed of un-exfoliated AG were removed. The obtained GO-QDs were dispersed in water for further study. To make a comparison, FG (CP, Aladdin Reagent Database Inc., Shanghai, China) was exfoliated via the same procedure. For investigating the exfoliating mechanism of AG, the exfoliating process was stopped at intercalation and oxidation steps, respectively. The corresponding intermediate products were isolated, characterized, and stored under appropriate conditions. The products obtained after intercalation by  $\text{H}_2\text{SO}_4$  are defined as AG-I and FG-I, respectively, and the products obtained after oxidation by  $\text{KMnO}_4$  are defined as AG-O and FG-O, respectively.

### 2.2. Preparation of GQDs with Different Functional Groups

For obtaining GQDs, 1 mg of the prepared GO-QDs was added into 10 mL of deionized water, and the mixture was placed into a sonic bath for 30 min to obtain a homogeneous solution. The solution was sealed in a Teflon-line autoclave at  $90^\circ\text{C}$ – $200^\circ\text{C}$  for 12 h. After cooling to room temperature, GQDs

were obtained. For obtaining GQDs modified with functional groups, different functional molecules can be added during the hydrothermal process. For example, modified GQDs of GQDs-NH<sub>3</sub>·H<sub>2</sub>O, GQDs-NaBH<sub>4</sub>, and GQDs-H<sub>3</sub>BO<sub>3</sub> were simply prepared by adding ammonia, NaBH<sub>4</sub>, and H<sub>3</sub>BO<sub>3</sub> as modifier during hydrothermal treatment, respectively.

### 2.3. Characterization

The crystalline phases of the samples were identified by using X-ray powder diffraction (XRD) techniques (Bruker D8 Advance diffractometer, Karlsruhe, Germany) operating with Cu K $\alpha$  radiation ( $\lambda = 0.15418$  nm) at a scan rate ( $2\theta$ ) of  $3^\circ \text{ min}^{-1}$ . The scan range is from  $10^\circ$  to  $70^\circ$ . The morphologies of the samples were characterized by using a field emission scanning electron microscope (SEM, Hitachi S4800, Tokyo, Japan), and a Tecnai G2 F30 S-Twin transmission electron microscope (TEM, FEI company, Hillsboro, OR, USA). The morphology and thickness of GO-QDs were obtained by an atomic force microscope (AFM, Cypher ES, Asylum Research, Oxford Instrument, Oxford, UK). Samples used for AFM characterization were prepared by dipping the piranha-cleaned silicon wafer substrate into their ethanolic suspensions. Raman spectra were recorded using a Raman microscopy (Horiba, LabRAM HR Evolution, Villeneuve-d'Ascq, France). Thermogravimetric analyses (TG) of samples were conducted using a thermal analyzer (NETZSCH, Selb, Germany). Samples were analyzed in the temperature range of  $25\text{--}790^\circ\text{C}$  under a flow of nitrogen. X-ray photoelectron spectroscopy (XPS) was carried out on a PHI-5000 Versa Probe instrument (ULVAC-PHI, Chigasaki, Japan) with Al K $\alpha$  X-ray source. The Fourier transform infrared spectra (FT-IR) of the samples were obtained with a PerkinElmer spectrum 100 (PerkinElmer, Waltham, MA, USA), in which KBr was used as diluents. PL lifetimes and quantum yield were investigated by LSP920 (Edinburgh Instruments, Corston, UK) using Xenon lamps (450 W).

### 2.4. Detection of Metal Ions in Water

Cu<sup>2+</sup> solution was prepared in advance with CuCl<sub>2</sub>, and then mixed with the above-mentioned GQDs-NH<sub>3</sub>·H<sub>2</sub>O in a certain proportion. Finally, a series of solution were obtained with a concentration of Cu<sup>2+</sup> in the range of  $0\text{--}100\ \mu\text{M}$ . The resulting solution was shaken well to ensure the complete reaction, and then its fluorescence emission is measured at the optimal excitation wavelength of 323 nm to detect the change of fluorescence intensity because of Cu<sup>2+</sup>. For detecting other metal ions, CuCl<sub>2</sub> was replaced by FeCl<sub>3</sub>, MnCl<sub>2</sub>, AgNO<sub>3</sub>, KCl, CuCl<sub>2</sub>, CaCl<sub>2</sub>, BaCl<sub>2</sub>, MgCl<sub>2</sub>, CdCl<sub>2</sub>, and ZnCl<sub>2</sub>, respectively.

## 3. Results and Discussion

### 3.1. Synthesis and Characterization of GO-QDs from AG

The exfoliating of AG was carried out by a modified Hummers' method, which is the most commonly used for the preparation of graphene oxide (GO) sheets [44]. TEM and AFM images in Figure 1a,b indicate that product synthesized from AG is composed of quantum dots with narrow size distribution. The average size of these GO-QDs is about 4.5 nm as calculated by counting 100 nanoparticles (Figure 1c). GO-QDs have an average thickness of  $\sim 3$  nm, which corresponds to only 2–3 layers of graphene sheets (Figure 1c). The yield of these GO-QDs is about 40 wt. % of raw AG. So, a large amount of GO-QDs can be obtained with AG precursor, and the concentration of GO-QDs aqueous solution can reach up to  $5\ \text{mg}\cdot\text{mL}^{-1}$  (Figure 1d). For comparison, FG were also adopted as precursors for preparing GO-QDs under the same conditions. Figure 1e shows that at low resolution the product synthesized from FG looks like a crumpled membrane with large size, which should be GO sheets. Small size quantum dots cannot be observed on this large crumpled membrane. If this product is further separated under 15,000 rpm for 30 min, large GO nanosheets are removed and small size GO nanosheets can be observed (Figure 1f). The size of these small GO nanosheets is mostly larger than 30 nm and not uniform, as well as the yield of these small GO sheets is less than 10 wt. % of

raw FG. Above results demonstrate that GO-QDs with high yield and high quality can be synthesized by using low cost AG.

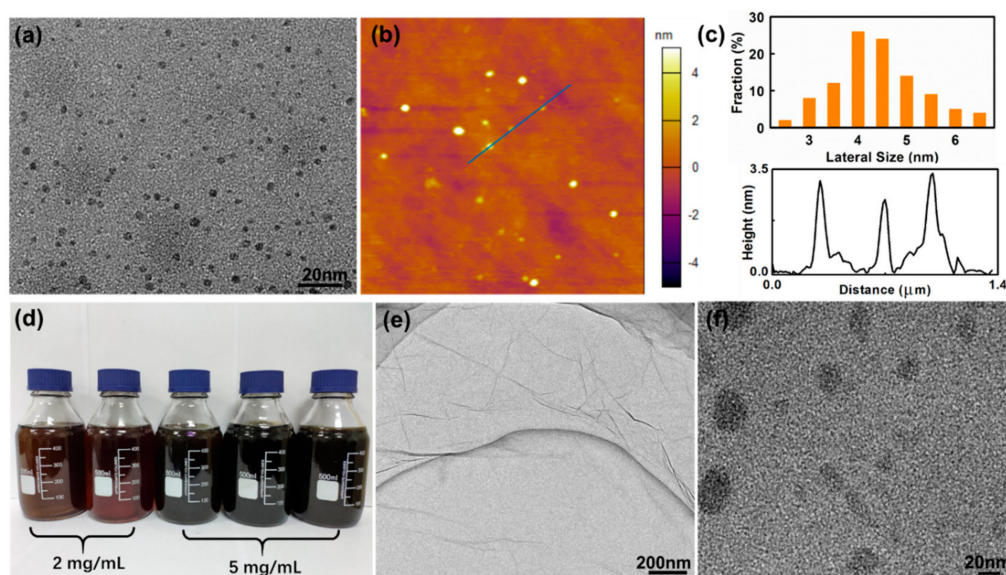


**Figure 1.** (a) Transmission electron microscope (TEM) and atomic force microscope (AFM). (b) Images of graphene oxide quantum dots (GO-QDs) synthesized from aphanitic graphite (AG). (c) Lateral size and height distribution. (d) Mass produced GO-QDs aqueous solution. (e) TEM image of GO synthesized from flake graphite (FG). (f) GO nanosheets synthesized from FG. (Separated at 15,000 rpm for 30 min).

### 3.2. Synthesis Mechanism of GO-QDs from AG

To understand the synthesis mechanism of GO-QDs from AG, the difference between AG and FG were compared first. The morphology difference between AG and FG can be obviously observed from their SEM images. Figure 2a indicates that FG has a large layered structure. The average length of these layers is about 35  $\mu\text{m}$ . Completely different from FG, AG has a particle structure (Figure 2b). The average diameter of AG particles is about 5  $\mu\text{m}$  (Figure 2c). It is noteworthy that each AG particle contains a large amount of small graphite nanocrystals with size of less than 10 nm as pointed in Figure 2d. These graphite nanocrystals are not fully developed graphite crystals during the formation period. If these small graphite nanocrystals are exfoliated, GQDs will be obtained directly without needing high-intensity or repeated cutting.

To further investigate the structural difference, XRD and Raman spectroscopy of AG and FG were characterized. Figure S1a shows XRD patterns of AG and FG. It can be observed that there are two strong peaks at  $26.5^\circ$  and  $54.6^\circ$  in the XRD pattern of FG, which is characteristic peaks of (002) and (004) of graphite materials [45]. In the XRD pattern of AG, the intensity of these peaks is quite weaker than that of FG, which suggests the low c-axis order and poor crystallinity of AG. The positions of characteristic peaks of AG are the same as that of FG and no other impurities are detected in AG, suggesting the graphite nature of AG but not amorphous coal. The Raman spectrum of FG in Figure S1b reveals their defect-free graphite nature due to the absence of D band signal. In AG, D band ( $1341\text{ cm}^{-1}$ ) is strong and  $I_D/I_G$  ratio is 0.48 attributing to smaller average size of  $\text{sp}^2$  domains in AG. The smaller the  $\text{sp}^2$  domain, the higher the edge concentration in AG is and the stronger the D band. These results are in accordance with the TEM and SEM results.

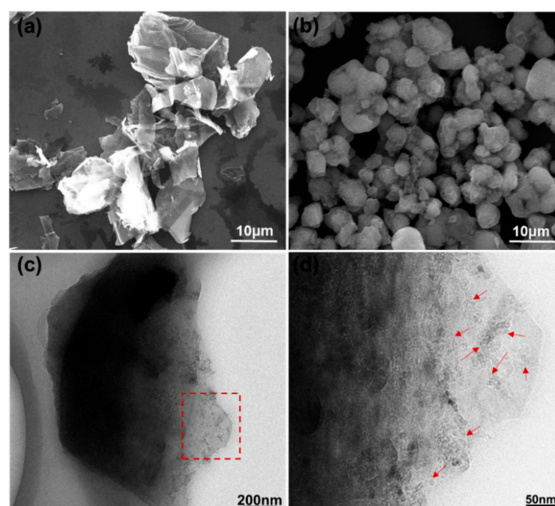


**Figure 2.** (a) SEM image of FG, (b–d) SEM and TEM images of aphanitic graphite (AG). The red arrows in Figure 2d point the small graphite nanocrystals.

Tour and co-workers showed that the formation of GO from bulk graphite by modified Hummers' method is a diffusive-controlled process [46]. Smaller-size flakes and lower crystalline graphite are oxidized significantly faster and more fully than the large and high crystalline flakes at same usage of oxidant. For investigating the mechanism in depth, the chemical and structural changes, which occurred during exfoliating of AG and FG, were monitored by XRD, Raman, FTIR, and TG analyses. The products obtained after intercalation by  $\text{H}_2\text{SO}_4$  are defined as AG-I and FG-I, respectively, and the products obtained after oxidation by  $\text{KMnO}_4$  are defined as AG-O and FG-O, respectively. Figure 3 show XRD patterns and Raman spectra of AG, AG-I, AG-O, FG, FG-I, and FG-O. The corresponding data are listed in Table 1.

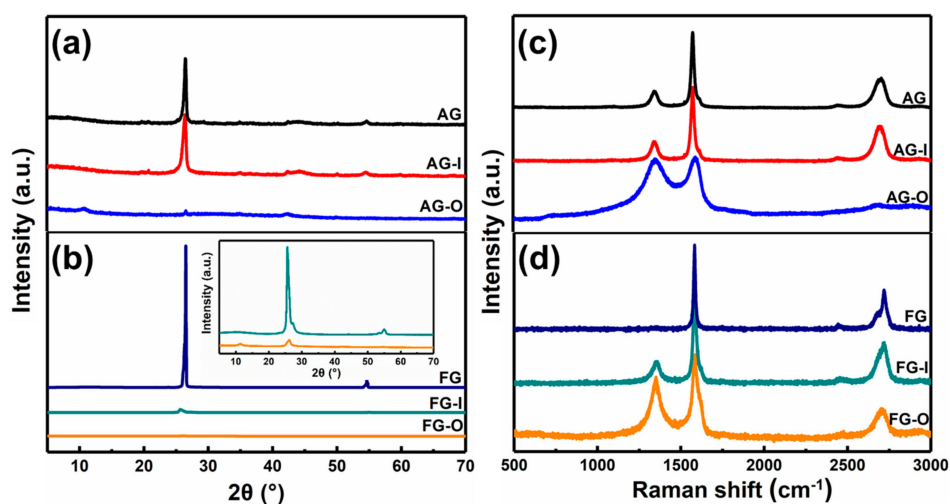


**Figure 3.** (a) XRD patterns and (c) Raman spectra of AG, AG-I, AG-O. (b) XRD patterns and (d) Raman spectra of FG, FG-I, and FG-O.

**Table 1.** Comparison of XRD and Raman data of AG and FG during exfoliating.

Measurements		Pristine	After Intercalation	After Oxidation
$2\theta(^{\circ})$	AG	26.5	26.4	10.7
	FG	26.5	25.7	11.3
$I_D/I_G$	AG	0.48	0.60	2.65
	FG	0	0.71	1.31

It can be observed that intercalation process has less effect on the structure of AG. However, for FG, after intercalation of  $\text{H}_2\text{SO}_4$ , the intensity of characteristic peak of (002) is dramatically decreased and  $I_{\text{D}}/I_{\text{G}}$  ratio increases to 0.71, indicating an increase of degree of disorders. The less effect of intercalation on AG is related to the more disorders of AG than FG. After oxidation, the characteristic peaks at  $26.5^\circ$  in AG and FG almost disappear and new peaks appear at  $10.71^\circ$  and  $11.34^\circ$ , respectively (Figure 3a,b). From Figure 3c,d and Table 1 it can be found that after oxidation  $I_{\text{D}}/I_{\text{G}}$  ratios of AG-O and FG-O all significantly increase compared with that of the corresponding precursors, indicating the destruction of conjugated  $\text{sp}^2$  networks. The  $I_{\text{D}}/I_{\text{G}}$  ratio of AG-O is much higher than that of FG-O, suggesting more oxygen-containing functional groups in AG-O than FG-O. The higher-degree oxidation of AG is also confirmed by FTIR and TG analyses in Figure 4. FG-O exhibits many vibration peaks of O–H stretch and bending at  $3422\text{ cm}^{-1}$  and  $1382\text{ cm}^{-1}$ , respectively, attributed to hydroxyl and phenolic groups, C=C stretch of unoxidized  $\text{sp}^2$  carbon domain at  $1622\text{ cm}^{-1}$ , C–O stretch at  $1235\text{ cm}^{-1}$  ascribed to phenols, ethers, and epoxy groups, and C–O stretch at  $1048$  and  $1111\text{ cm}^{-1}$  attributed to hydroxyl groups (Figure 4a). All these mentioned peaks can be observed in AG-O, and they are stronger than those in FG-O. Additionally, C=O stretch at  $1723\text{ cm}^{-1}$  attributed to carboxyl and carbonyl groups is detected in AG-O. TG analysis indicates that both FG-O and AG-O show two significant weight losses ( $\sim 10$  and  $\sim 17\%$ ) near  $100^\circ\text{C}$  and ( $\sim 20$  and  $\sim 29\%$ ) in the range of  $150\text{--}300^\circ\text{C}$ , owing to the evaporation of the trapped water molecules and thermal decomposition of oxygen-containing functional groups in the samples, respectively (Figure 4b). All above results demonstrate that AG has a higher degree oxidation. The oxidation is complete and homogeneous due to shorter diffusion path for oxidant between AG layers, which is difficult to achieve for FG at the same condition because of the diffusion resistance between large layers. A large amount of GO-QDs can be obtained by exfoliation of fully oxidized AG-O without further high-strength cutting (Figure 5).

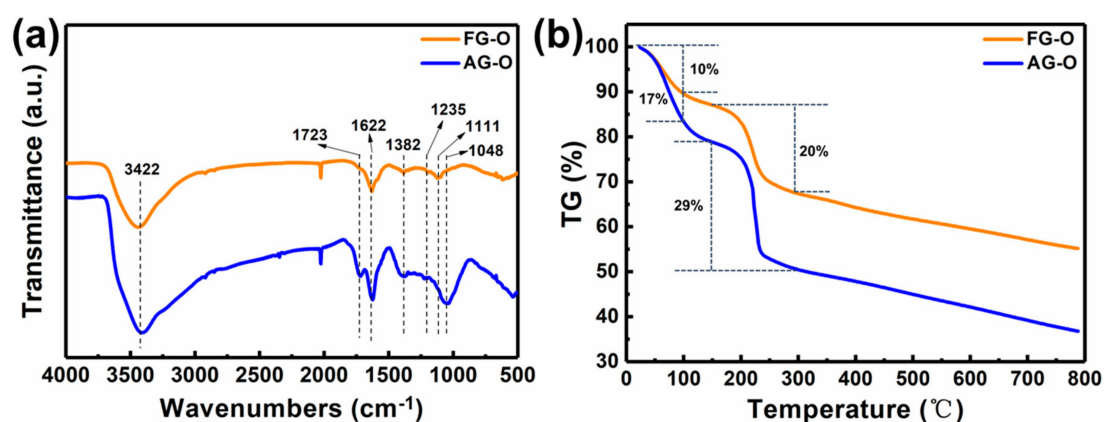


Figure 4. (a) FTIR spectra and (b) TG curves of FG-O and AG-O.

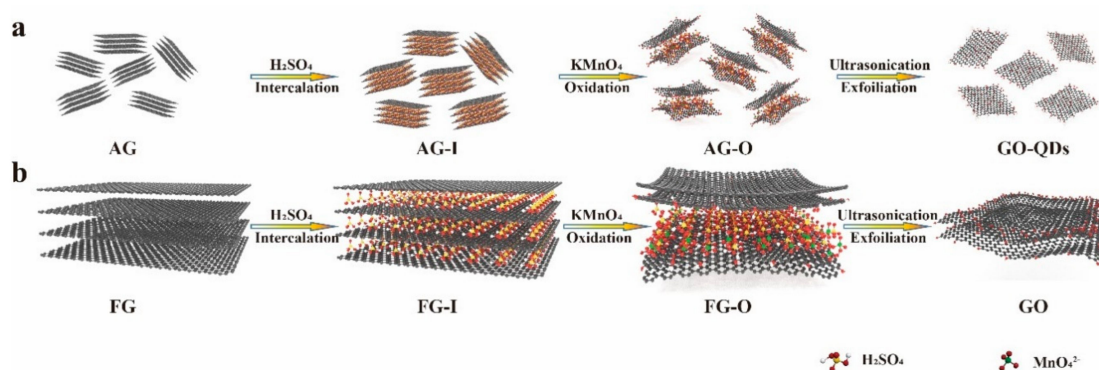
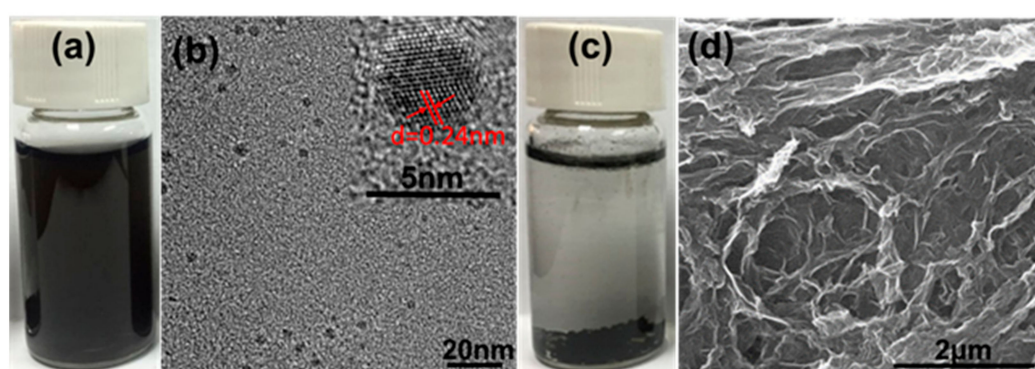


Figure 5. Schematic of the exfoliating of (a) AG and (b) FG with the same amount of intercalator and oxidizer.

### 3.3. Modification of GO-QDs and Their Applications

The obtained large amount of GO-QDs from AG can be used as precursor for GQDs with different properties. If GO-QDs are treated in pure water by hydrothermal method, brown GO-QDs turn into black GQDs. These GQDs can keep in good dispersion in water even after standing for 6 months (Figure 6a). TEM image in Figure 6b further confirms the monodispersing of GQDs. The concentration of the obtained GQDs dispersion can reach to 1 mg/ml. HRTEM image of GQDs was measured as shown in Figure 6b inset. The lattice distance of 0.24 nm is observed, suggesting the crystalline nature of GQDs. Controlled experiment was carried out by treating the product synthesized from FG at the same condition. The picture in Figure 6c indicates that after hydrothermal treatment the black agglomerate deposits at the bottom. During hydrothermal treatment, the large GO sheets (Figure 1e) with rich -OH and -COOH groups in the plane are very easy to connect with each other and form a 3D structure by the interaction of hydrogen bond [47] (Figure 6d).



**Figure 6.** (a) Picture and (b) TEM and HRTEM (inset) images of GQDs by hydrothermal treatment of GO-QDs. (c) Picture and (d) SEM image of product after hydrothermal treatment of GO.

XPS test further confirm the reduction of GO-QDs during hydrothermal treatment. Comparing with GO-QDs (Figure S2a), the binding energy peaks of GQDs do not shift, but their intensities drastically change. The intensities of oxygen-containing functional groups such as -C-O, -C=O, and -O-C=O significantly decrease. The peak intensity of C-C increases (Figure S2b). These results suggest the reduction of GO-QDs during hydrothermal treatment. GO-QDs has an orange-emission at 595 nm (Figure 7). After the removal of oxygen-containing functional groups, GQDs almost have no fluorescence emission. While a series of GQDs with different fluorescence properties can be easily synthesized from GO-QDs by adding modifiers during hydrothermal treatment. For example, three kinds of soluble fluorescent GQDs could be obtained by adding ammonia,  $\text{NaBH}_4$ , and  $\text{H}_3\text{BO}_3$  as modifier during hydrothermal treatment, respectively. These fluorescent GQDs are defined as GQDs- $\text{NH}_3\cdot\text{H}_2\text{O}$ , GQDs- $\text{NaBH}_4$  and GQDs- $\text{H}_3\text{BO}_3$ , respectively. These modified GQDs exhibit fluorescence emission at 425 nm, 435 nm, and 539 nm, respectively (Figure 7). Therefore, GQDs with different fluorescence properties for specific application requirements can be synthesized by AG in a large scale and its quality and quantity can be guaranteed by the special precursor. For example, the lifetime of GO-QDs is 1.07 ns and that of GQDs- $\text{NH}_3\cdot\text{H}_2\text{O}$  is 5.98 ns. Meanwhile, the quantum yield of GQDs- $\text{NH}_3\cdot\text{H}_2\text{O}$  (9.7%) is about twenty-five times as much as that of GO-QDS (0.4%) (Figure 8a and Table 2). After modification, the size of GQDs- $\text{NH}_3\cdot\text{H}_2\text{O}$  is almost the same as that of GO-QDs (Figure S3a). FTIR spectrum of GQDs- $\text{NH}_3\cdot\text{H}_2\text{O}$  demonstrates obvious N-H stretching vibration peaks in the range of  $3300\text{--}3600\text{ cm}^{-1}$ , N-H bending peak at  $1655\text{ cm}^{-1}$  and C-H stretching vibration peak at  $1412\text{ cm}^{-1}$  (Figure S3b). These results indicate the successful modification of GO-QDs by  $\text{NH}_3\cdot\text{H}_2\text{O}$ . GQDs- $\text{NH}_3\cdot\text{H}_2\text{O}$  with higher quantum yield can be used as fluorescence probe for detecting metal ions in water. The results indicate that GQDs- $\text{NH}_3\cdot\text{H}_2\text{O}$  has a high selectivity for copper ions ( $\text{Cu}^{2+}$ ) (Figure 8b). Figure 8c displays the PL intensity spectra of GQDs- $\text{NH}_3\cdot\text{H}_2\text{O}$  with different concentration of  $\text{Cu}^{2+}$  at 323 nm excitation. It can be clearly observed that the fluorescence quenching

of GQDs-NH<sub>3</sub>·H<sub>2</sub>O is naturally increasing with the increasing of Cu<sup>2+</sup> concentration. The modified plot in Figure 8d shows the relationship of F/F<sub>0</sub> and Cu<sup>2+</sup> concentration. There is a distinct linear relationship between quenched PL intensity ( $\Delta F/F_0$ ) and Cu<sup>2+</sup> concentration in the range of 5  $\mu$ M to 25  $\mu$ M (Inset in Figure 8d). The limitation of detection can reach up to 0.4  $\mu$ M, which is enough to satisfy the demand in detection for Cu<sup>2+</sup> in wastewater.

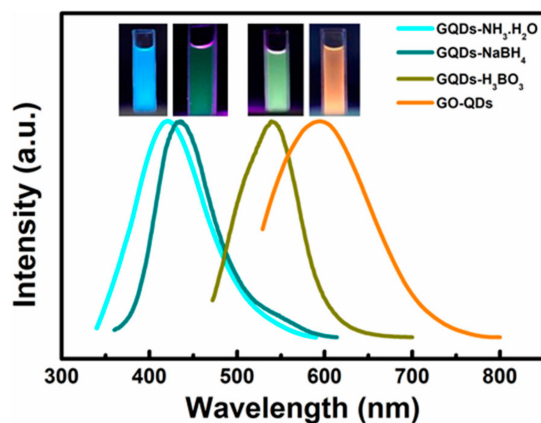


**Figure 7.** PL spectra of GO-QDs, GQDs-NH<sub>3</sub>·H<sub>2</sub>O, GQDs-NaBH<sub>4</sub> and GQDs-H<sub>3</sub>BO<sub>3</sub> excited at 323 nm. The insets are their corresponding digital photographs ( $\lambda_{\text{exc}} = 365$  nm).

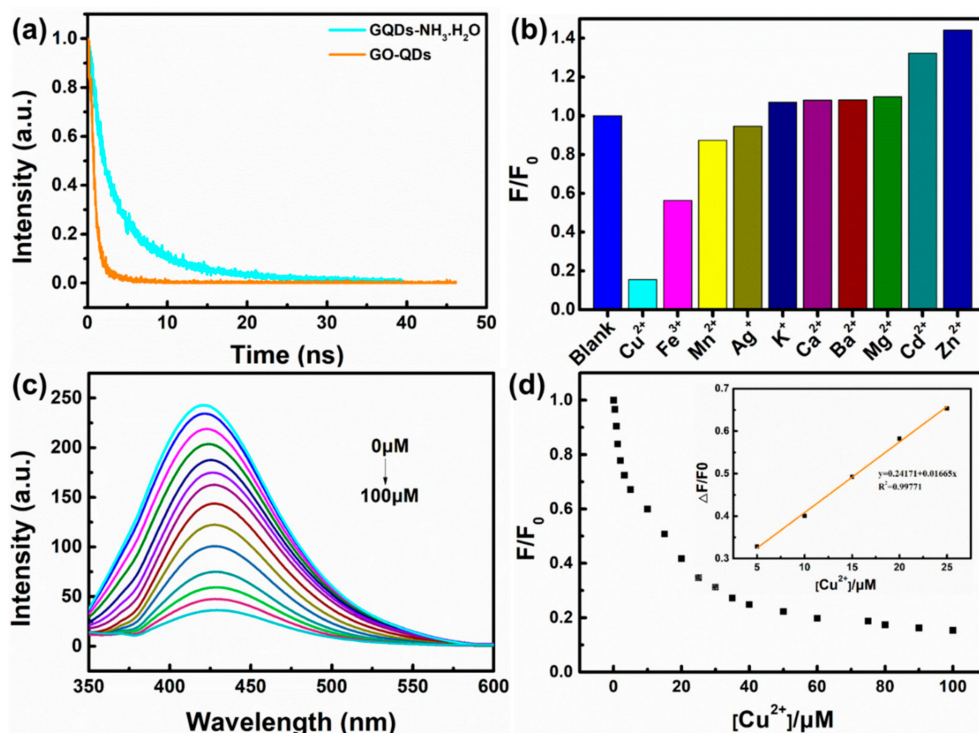


**Figure 8.** (a) Time resolved PL decay curves of GO-QDs and GQDs-NH<sub>3</sub>·H<sub>2</sub>O. (b) The effect of different metal ions on the PL intensity of GQDs-NH<sub>3</sub>·H<sub>2</sub>O, (c) PL quenching of GQDs-NH<sub>3</sub>·H<sub>2</sub>O with different concentration of Cu<sup>2+</sup>, and (d) the relationship of F/F<sub>0</sub> and Cu<sup>2+</sup> concentration.

**Table 2.** Exponential fitting results for time resolved PL decay curves of GO-QDs and GQDs-NH<sub>3</sub>·H<sub>2</sub>O.

Samples	$\tau_1$ (ns)	A <sub>1</sub> (%)	$\tau_2$ (ns)	A <sub>2</sub> (%)	Lifetime(ns)
GO-QDs	0.6056	75.95	2.5346	24.05	1.07 ns
GQDs-NH <sub>3</sub> ·H <sub>2</sub> O	2.1349	36.59	8.1989	63.41	5.98 ns

#### 4. Conclusions

In conclusion, AG was used for the synthesis of QGDs for the first time. Comparing with FG, the merits of AG as precursor for QGDs is as follows: (i) AG is low cost, (ii) the synthesis process does not need high-strength cutting step, (iii) the size of obtained QGDs is uniform, high yielding (~40%), and of good quality, (iv) can be easily modified according to the request of applications. It is believed that these QGDs synthesized by AG as precursor can be a candidate for graphene-based tunable luminescent material in many potential fields.

**Supplementary Materials:** The following are available online at <http://www.mdpi.com/2079-4991/10/2/375/s1>. Figure S1: (a) XRD patterns and (b) Raman spectra of AG and FG. Figure S2: XPS patterns of GO-QDs (a) and QGDs (b). Figure S3: (a) TEM image of QGDs-NH<sub>3</sub>·H<sub>2</sub>O and (b) FTIR spectra of QGDs-NH<sub>3</sub>·H<sub>2</sub>O and GO-QDs.

**Author Contributions:** S.S. and J.Y. conceived the idea of experiment; J.W., Z.W., and Z.D. performed the experiments; S.S., J.W., Z.W., Z.D., and Z.T. discussed the results; S.S. and Z.W. wrote the original draft; S.S. and J.W. wrote, reviewed, and edited the manuscript. All authors have read and agreed to the published version of the manuscript.

**Funding:** This research was funded by Shanghai Scientific and Technological Innovation Project (19JC1410402), Shanghai Nature Science Foundation (16ZR1423400, 18ZR1426400), Shanghai Municipal Science and Technology Commission (16JC402200, 16060502300 and 18511110600) and the Innovation Program of Shanghai Municipal Education Commission (2019-01-07-00-07-E00015).

**Conflicts of Interest:** The authors declare no conflict of interest.

#### References

1. Stankovich, S.; Dikin, D.A.; Piner, R.D.; Kohlhaas, K.A.; Kleinhammes, A.; Jia, Y.; Wu, Y.; Nguyen, S.T.; Ruoff, R.S. Synthesis of graphene-based nanosheets via chemical reduction of exfoliated graphite oxide. *Carbon* **2007**, *45*, 1558–1565. [CrossRef]
2. Geim, A.K.; Novoselov, K.S. The rise of graphene. *Nat. Mater.* **2007**, *6*, 183–191. [CrossRef] [PubMed]
3. Lee, C.; Wei, X.D.; Kysar, J.W.; Hone, J. Measurement of the elastic properties and intrinsic strength of monolayer graphene. *Science* **2008**, *321*, 385–388. [CrossRef] [PubMed]
4. Liu, Y.; Dong, X.; Chen, P. Biological and chemical sensors based on graphene materials. *Chem. Soc. Rev.* **2012**, *41*, 2283–2307. [CrossRef] [PubMed]
5. Perreault, F.; Fonseca de Faria, A.; Elimelech, M. Environmental applications of graphene-based nanomaterials. *Chem. Soc. Rev.* **2015**, *44*, 5861–5896. [CrossRef] [PubMed]
6. Raccichini, R.; Varzi, A.; Passerini, S.; Scrosati, B. The role of graphene for electrochemical energy storage. *Nat. Mater.* **2015**, *14*, 271–279. [CrossRef]
7. Abraham, J.; Vasu, K.S.; Williams, C.D.; Gopinadhan, K.; Su, Y.; Cherian, C.T.; Dix, J.; Prestat, E.; Haigh, S.J.; Grigorieva, I.V.; et al. Tunable sieving of ions using graphene oxide membranes. *Nat. Nanotechnol.* **2017**, *12*, 546–550. [CrossRef]
8. Sun, J.; Lee, H.W.; Pasta, M.; Yuan, H.; Zheng, G.; Sun, Y.; Li, Y.; Cui, Y. A phosphorene-graphene hybrid material as a high-capacity anode for sodium-ion batteries. *Nat. Nanotechnol.* **2015**, *10*, 980–985. [CrossRef]
9. Suvarnaphaet, P.; Pechprasarn, S. Graphene-Based Materials for Biosensors: A Review. *Sensors* **2017**, *17*, 2161. [CrossRef]
10. Liao, L.; Peng, H.; Liu, Z. Chemistry makes graphene beyond graphene. *J. Am. Chem. Soc.* **2014**, *136*, 12194–12200. [CrossRef]
11. Bartolomeo, A.D.; Luongo, G.; Iemmo, L.; Urban, F.; Giubileo, F. Graphene-Silicon Schottky diodes for photodetection. *IEEE Trans. Nanotechnol.* **2018**, *17*, 1133–1137. [CrossRef]
12. Huang, Y.; Cheng, H.; Shi, G.; Qu, L. Highly Efficient Moisture-Triggered Nanogenerator Based on Graphene Quantum Dots. *ACS Appl. Mater. Interfaces* **2017**, *9*, 38170–38175. [CrossRef] [PubMed]
13. Li, X.; Rui, M.; Song, J.; Shen, Z.; Zeng, H. Carbon and Graphene Quantum Dots for Optoelectronic and Energy Devices: A Review. *Adv. Funct. Mater.* **2015**, *25*, 4929–4947. [CrossRef]
14. Zhu, S.; Zhang, J.; Qiao, C.; Tang, S.; Li, Y.; Yuan, W.; Li, B.; Tian, L.; Liu, F.; Hu, R.; et al. Strongly green-photoluminescent graphene quantum dots for bioimaging applications. *Chem. Commun.* **2011**, *47*, 6858–6860. [CrossRef]

15. Zheng, P.; Wu, N. Fluorescence and Sensing Applications of Graphene Oxide and Graphene Quantum Dots: A Review. *Chem. Asian J.* **2017**, *12*, 2343–2353. [[CrossRef](#)]
16. Kellarakis, A. Graphene quantum dots: In the crossroad of graphene, quantum dots and carbogenic nanoparticles. *Curr. Opin. Colloid Interface Sci.* **2015**, *20*, 354–361. [[CrossRef](#)]
17. Xu, H.; Zhang, L.; Ding, Z.; Hu, J.; Liu, J.; Liu, Y. Edge-functionalized graphene quantum dots as a thickness-insensitive cathode interlayer for polymer solar cells. *Nano Res.* **2018**, *11*, 4293–4301. [[CrossRef](#)]
18. Wang, Z.; Zeng, H.; Sun, L. Graphene quantum dots: versatile photoluminescence for energy, biomedical, and environmental applications. *J. Mater. Chem. C* **2015**, *3*, 1157–1165. [[CrossRef](#)]
19. Li, K.; Liu, W.; Ni, Y.; Li, D.; Lin, D.; Su, Z.; Wei, G. Technical synthesis and biomedical applications of graphene quantum dots. *J. Mater. Chem. B* **2017**, *5*, 4811–4826. [[CrossRef](#)]
20. Zhou, S.; Xu, H.; Gan, W.; Yuan, Q. Graphene quantum dots: recent progress in preparation and fluorescence sensing applications. *RSC Adv.* **2016**, *6*, 110775–110788. [[CrossRef](#)]
21. Zheng, X.T.; Ananthanarayanan, A.; Luo, K.Q.; Chen, P. Glowing graphene quantum dots and carbon dots: properties, syntheses, and biological applications. *Small* **2015**, *11*, 1620–1636. [[CrossRef](#)] [[PubMed](#)]
22. Tang, L.B.; Ji, R.B.; Cao, X.K.; Lin, J.Y.; Jiang, H.X.; Li, X.M.; Teng, K.S.; Luk, C.M.; Zeng, S.J.; Hao, J.H.; et al. Deep Ultraviolet Photoluminescence of Water-Soluble Self-Passivated Graphene Quantum Dots. *ACS Nano* **2012**, *6*, 5102–5110. [[CrossRef](#)] [[PubMed](#)]
23. Dong, Y.; Shao, J.; Chen, C.; Li, H.; Wang, R.; Chi, Y.; Lin, X.; Chen, G. Blue luminescent graphene quantum dots and graphene oxide prepared by tuning the carbonization degree of citric acid. *Carbon* **2012**, *50*, 4738–4743. [[CrossRef](#)]
24. Liu, R.; Wu, D.; Feng, X.; Mullen, K. Bottom-up fabrication of photoluminescent graphene quantum dots with uniform morphology. *J. Am. Chem. Soc.* **2011**, *133*, 15221–15223. [[CrossRef](#)] [[PubMed](#)]
25. Yan, X.; Li, B.S.; Li, L.S. Colloidal Graphene Quantum Dots with Well-Defined Structures. *Acc. Chem. Res.* **2013**, *46*, 2254–2262. [[CrossRef](#)]
26. Yang, S.; Sun, J.; Li, X.; Zhou, W.; Wang, Z.; He, P.; Ding, G.; Xie, X.; Kang, Z.; Jiang, M. Large-scale fabrication of heavy doped carbon quantum dots with tunable-photoluminescence and sensitive fluorescence detection. *J. Mater. Chem. A* **2014**, *2*, 8660. [[CrossRef](#)]
27. Pan, D.; Zhang, J.; Li, Z.; Wu, M. Hydrothermal route for cutting graphene sheets into blue-luminescent graphene quantum dots. *Adv. Mater.* **2010**, *22*, 734–738. [[CrossRef](#)]
28. Shin, Y.; Park, J.; Hyun, D.; Yang, J.; Lee, J.H.; Kim, J.H.; Lee, H. Acid-free and oxone oxidant-assisted solvothermal synthesis of graphene quantum dots using various natural carbon materials as resources. *Nanoscale* **2015**, *7*, 5633–5637. [[CrossRef](#)]
29. Ahirwar, S.; Mallick, S.; Bahadur, D. Electrochemical method to prepare graphene quantum dots and graphene oxide quantum dots. *ACS Omega* **2017**, *2*, 8343–8353. [[CrossRef](#)]
30. Li, Y.; Hu, Y.; Zhao, Y.; Shi, G.; Deng, L.; Hou, Y.; Qu, L. An electrochemical avenue to green-luminescent graphene quantum dots as potential electron-acceptors for photovoltaics. *Adv. Mater.* **2011**, *23*, 776–780. [[CrossRef](#)]
31. Ananthanarayanan, A.; Wang, X.; Routh, P.; Sana, B.; Lim, S.; Kim, D.-H.; Lim, K.-H.; Li, J.; Chen, P. Facile Synthesis of Graphene Quantum Dots from 3D Graphene and their Application for Fe<sup>3+</sup> Sensing. *Adv. Funct. Mater.* **2014**, *24*, 3021–3026. [[CrossRef](#)]
32. Zhou, X.J.; Zhang, Y.; Wang, C.; Wu, X.C.; Yang, Y.Q.; Zheng, B.; Wu, H.X.; Guo, S.W.; Zhang, J.Y. Photo-Fenton Reaction of Graphene Oxide: A new strategy to prepare graphene quantum dots for DNA cleavage. *ACS Nano* **2012**, *6*, 6592–6599. [[CrossRef](#)] [[PubMed](#)]
33. Li, Z.; Li, Z.; Wu, Y.; Nan, J.; Wang, H.; Zhang, X.; Zhang, J.; Yang, B. Tuning the bandgap of graphene quantum dots by gold nanoparticle-assisted O<sub>2</sub> plasma etching. *RSC Adv.* **2016**, *6*, 97853–97860. [[CrossRef](#)]
34. El-Hnayn, R.; Canabady-Rochelle, L.; Desmarests, C.; Balan, L.; Rinnert, H.; Joubert, O.; Medjahdi, G.; Ouada, H.B.; Schneider, R. One-step synthesis of diamine-functionalized graphene quantum dots from graphene oxide and their chelating and antioxidant activities. *Nanomaterials* **2020**, *10*, 104. [[CrossRef](#)]
35. Chen, G.; Zhuo, Z.; Ni, K.; Kim, N.Y.; Zhao, Y.; Chen, Z.; Xiang, B.; Yang, L.; Zhang, Q.; Lee, Z.; et al. Rupturing C60 molecules into graphene-oxide-like quantum dots: structure, photoluminescence, and catalytic application. *Small* **2015**, *11*, 5296–5304. [[CrossRef](#)]
36. Zhang, C.; Li, J.; Zeng, X.; Yuan, Z.; Zhao, N. Graphene quantum dots derived from hollow carbon nano-onions. *Nano Res.* **2018**, *11*, 174–184. [[CrossRef](#)]

37. Peng, J.; Gao, W.; Gupta, B.K.; Liu, Z.; Romero-Aburto, R.; Ge, L.; Song, L.; Alemany, L.B.; Zhan, X.; Gao, G.; et al. Graphene quantum dots derived from carbon fibers. *Nano Lett.* **2012**, *12*, 844–849. [[CrossRef](#)]
38. Ye, R.; Xiang, C.; Lin, J.; Peng, Z.; Huang, K.; Yan, Z.; Cook, N.P.; Samuel, E.L.; Hwang, C.C.; Ruan, G.; et al. Coal as an abundant source of graphene quantum dots. *Nat. Commun.* **2013**, *4*, 2943–2948. [[CrossRef](#)]
39. Dong, Y.; Lin, J.; Chen, Y.; Fu, F.; Chi, Y.; Chen, G. Graphene quantum dots, graphene oxide, carbon quantum dots and graphite nanocrystals in coals. *Nanoscale* **2014**, *6*, 7410–7415. [[CrossRef](#)]
40. Liu, F.; Jang, M.H.; Ha, H.D.; Kim, J.H.; Cho, Y.H.; Seo, T.S. Facile synthetic method for pristine graphene quantum dots and graphene oxide quantum dots: origin of blue and green luminescence. *Adv. Mater.* **2013**, *25*, 3657–3662. [[CrossRef](#)]
41. Wang, Z.; Yu, J.; Zhang, X.; Li, N.; Liu, B.; Li, Y.; Wang, Y.; Wang, W.; Li, Y.; Zhang, L.; et al. Large-scale and controllable synthesis of graphene quantum dots from rice husk biomass: a comprehensive utilization strategy. *ACS Appl. Mater. Interfaces* **2016**, *8*, 1434–1439. [[CrossRef](#)] [[PubMed](#)]
42. Lin, S.F.; Liu, F.X.; Chen, G.H. Effective production of nano-sized graphene via straight-forward exfoliation of microcrystalline graphite. *RSC Adv.* **2014**, *4*, 45885–45889. [[CrossRef](#)]
43. Wang, J.; Huang, J.; Yan, R.; Wang, F.; Cheng, W.; Guo, Q.; Wang, J. Graphene microsheets from natural microcrystalline graphite minerals: scalable synthesis and unusual energy storage. *J. Mater. Chem. A* **2015**, *3*, 3144–3150. [[CrossRef](#)]
44. Han, Z.; Tang, Z.; Li, P.; Yang, G.; Zheng, Q.; Yang, J. Ammonia solution strengthened three-dimensional macro-porous graphene aerogel. *Nanoscale* **2013**, *5*, 5462–5467. [[CrossRef](#)]
45. Li, Z.Q.; Lu, C.J.; Xia, Z.P.; Zhou, Y.; Luo, Z. X-ray diffraction patterns of graphite and turbostratic carbon. *Carbon* **2007**, *45*, 1686–1695. [[CrossRef](#)]
46. Dimiev, A.M.; Tour, J.M. Mechanism of graphene oxide formation. *ACS Nano* **2014**, *8*, 3060–3068. [[CrossRef](#)]
47. Wasalathilake, K.C.; Galpaya, D.G.D.; Ayoko, G.A.; Yan, C. Understanding the structure-property relationships in hydrothermally reduced graphene oxide hydrogels. *Carbon* **2018**, *137*, 282–290. [[CrossRef](#)]



© 2020 by the authors. Licensee MDPI, Basel, Switzerland. This article is an open access article distributed under the terms and conditions of the Creative Commons Attribution (CC BY) license (<http://creativecommons.org/licenses/by/4.0/>).